Application of modified integration rule to time-domain finite-element acoustic simulation of rooms

Okuzono, Takeshi
Otsuru, Toru
Tomiku, Reiji
Okamoto, Noriko

(Citation)
Journal of the Acoustical Society of America,132(2):804-813

(Issue Date)
2012-08

(Resource Type)
journal article

(Version)
Version of Record

Application of modified integration rule to time-domain finite-element acoustic simulation of rooms

Takeshi Okuzono, Toru Otsuru, Reiji Tomiku, and Noriko Okamoto

Citation: The Journal of the Acoustical Society of America **132**, 804 (2012); doi: 10.1121/1.4730920
View online: https://doi.org/10.1121/1.4730920
View Table of Contents: https://asa.scitation.org/toc/jas/132/2
Published by the Acoustical Society of America

Application of modified integration rule to time-domain finite-element acoustic simulation of rooms

Takeshi Okuzono[a)]
Faculty of Engineering, Oita University, 700 Dannoharu, Oita 870-1192, Japan

Toru Otsuru and Reiji Tomiku
Department of Architecture and Mechatronics, Architecture Course, Faculty of Engineering, Oita University, 700 Dannoharu, Oita 870-1192, Japan

Noriko Okamoto
Department of Architecture, Ariake National College of Technology, 150 Higashihagio-Machi, Omuta Fukuoka 836-8585, Japan

(Received 19 October 2011; revised 4 June 2012; accepted 7 June 2012)

The applicability of the modified integration rule for time-domain finite-element analysis is tested in sound field analysis of rooms involving rectangular elements, distorted elements, and finite impedance boundary conditions. Dispersion error analysis in three dimensions is conducted to evaluate the dispersion error in time-domain finite-element analysis using eight-node hexahedral elements. The results of analysis confirmed that fourth-order accuracy with respect to dispersion error is obtainable using the Fox–Goodwin method (FG) with a modified integration rule, even for rectangular elements. The stability condition in three-dimensional analysis using the modified integration rule is also presented. Numerical experiments demonstrate that FG with a modified integration rule performs much better than FG with the conventional integration rule for problems with rectangular elements, distorted elements, and with finite impedance boundary conditions. Further, as another advantage, numerical results revealed that the use of modified integration rule engenders faster convergence of the iterative solver than a conventional rule for problems with the same degrees of freedom.
[http://dx.doi.org/10.1121/1.4730920]

PACS number(s): 43.55.Ka, 43.55.Br [NX] Pages: 804–813

I. INTRODUCTION

Wave-based numerical methods, such as finite-difference time-domain method,[1–3] finite-element method (FEM),[4–6] and boundary-element method,[7] are indispensable tools used to predict a sound-field accurately in an architectural space with complicated boundary conditions. Time-domain finite-element method (TD-FEM), which is FEM with direct time integration such as Newmark β method,[8] is a powerful time-domain wave-based numerical method used in the field of architectural acoustics.[9,10] TD-FEM presents advantages in accuracy and flexibility of geometrical modeling, but this method incurs discretization error, called dispersion error, which is known as an error in wave velocity. Because of the error, the numerical wave velocity at each frequency differs from the exact wave velocity. Moreover, the error magnitude is dependent on the direction of wave propagation in multidimensional analysis.

In time-domain finite-element (TD-FE) analysis, discretization of both space and time, which maintain dispersion error within acceptable levels, is required to yield a reliable result. It engenders the solution of a large-scale linear system of equations at each time step when a practical sized room and/or practical frequency range is considered. Because the solution is computationally expensive, reduction of dispersion error is invaluable to realize efficient prediction of the sound fields, which engenders a decrease in the degrees of freedom (DOF) of the finite element (FE) model to obtain a result with an equivalent level of accuracy.

Some methods are available to reduce the dispersion error in TD-FE analysis, such as the dispersion-corrected explicit time integration scheme,[11] modified integration rule (MIR),[12] and high-order FEs.[13,14] Among them, MIR, proposed by Yue and Guddati,[12] is an effective and simple method of reducing dispersion error for low-order elements, which is proposed for both implicit and explicit TD-FEM using bilinear quadrilateral elements in two dimensions. In fact, MIR can reduce the dispersion error at all directions of wave propagation simply by modifying the numerical integration points of element mass and stiffness matrices, and TD-FEM with MIR has fourth-order accuracy with respect to the dispersion error. However, when MIR is applied to the sound field analysis of an architectural space, some problems remain in its application range. Yue and Guddati presented that MIR cannot significantly reduce dispersion error for rectangular elements, although the error for square elements can be reduced. Moreover, the MIR performance on sound field analyses with distorted elements and with finite impedance boundary conditions has not been fully examined. In Ref. 12, although only the performance of the explicit method with MIR is tested on a distorted mesh, the method

[a)]Author to whom correspondence should be addressed. Electronic mail: okuzono@oita-u.ac.jp

 0001-4966/2012/132(2)/804/10/$30.00

of determining a key parameter in the MIR (i.e., the size of a square element) is unclear for a distorted mesh. An architectural space typically has complicated boundary conditions. Therefore, extension of the application range of MIR for problems with rectangular and distorted elements, as well as finite impedance boundary conditions, is desired. In addition, although MIR is directly applicable to three-dimensional analysis, dispersion error analysis in three dimensions has not been reported in the literature. To determine the accuracy of FE analysis using MIR in three dimensions and to provide a basis for mesh generation, as well as time resolution, dispersion analysis is beneficial.

As described in this paper, the MIR is applied to sound field analysis of rooms by TD-FEM using eight-node hexahedral elements. The main purpose of this study is to demonstrate the applicability of the MIR to sound field analysis of rooms involving rectangular elements, distorted elements and finite impedance boundary conditions, to realize the efficient prediction of large-scale sound fields of rooms with complicated boundary conditions. Dispersion error analysis in three dimensions is performed and applicability of the MIR is tested for sound field analysis with rectangular elements and distorted elements, as well as finite impedance boundary conditions.

II. THEORY

A. TD-FEM for sound field analysis of rooms

We consider a three-dimensional sound field Ω (air density: ρ, speed of sound: c) with an impedance boundary surface and with a vibrating surface. Following standard FE discretization based on the principle of minimum potential energy, the following semi-discretized equation in a time domain is derived:

$$\boldsymbol{M}\ddot{\boldsymbol{p}} + c^2\boldsymbol{K}\boldsymbol{p} + c\boldsymbol{C}\dot{\boldsymbol{p}} = \rho c^2 \dot{v}_n \boldsymbol{W}, \tag{1}$$

where $\boldsymbol{M}$, $\boldsymbol{K}$, and $\boldsymbol{C}$, respectively, denote the global mass matrix, global stiffness matrix, and global dissipation matrix. Further, $\boldsymbol{p}$, v_n, and $\boldsymbol{W}$, respectively, denote sound pressure vector, velocity of vibration, and distribution vector. The global matrices are obtained by assembling the element stiffness matrix, $\boldsymbol{k}_e$, the element mass matrix, $\boldsymbol{m}_e$ and the element dissipation matrix, $\boldsymbol{c}_e$ defined as

$$\boldsymbol{k}_e = \int_{\Omega_e} \nabla \boldsymbol{N}^T \nabla \boldsymbol{N} d\Omega, \tag{2}$$

$$\boldsymbol{m}_e = \int_{\Omega_e} \boldsymbol{N}^T \boldsymbol{N} d\Omega, \tag{3}$$

$$\boldsymbol{c}_e = \frac{1}{z_n}\int_{\Gamma_e} \boldsymbol{N}^{\mathrm{T}} \boldsymbol{N} d\Gamma. \tag{4}$$

Here, $\boldsymbol{N}$ and z_n, respectively, represent the shape function and normalized acoustic impedance ratio. Ω_e and Γ_e, respectively, denote the region of an element and surface area of an element to be integrated.

In the time domain, Newmark β method is used to solve Eq. (1). As an initial condition, if $\boldsymbol{p}^n$, $\dot{\boldsymbol{p}}^n$, and $\ddot{\boldsymbol{p}}^n$ at time $t = n\Delta t$ are known, then $\boldsymbol{p}^{(n+1)}$ and $\dot{\boldsymbol{p}}^{(n+1)}$ can be given as

$$\boldsymbol{p}^{(n+1)} = \boldsymbol{p}^n + \Delta t \dot{\boldsymbol{p}}^n + \Delta t^2 \left(\frac{1}{2} - \beta\right)\ddot{\boldsymbol{p}}^n + \Delta t^2 \beta \ddot{\boldsymbol{p}}^{(n+1)}, \tag{5}$$

$$\dot{\boldsymbol{p}}^{(n+1)} = \dot{\boldsymbol{p}}^n + \Delta t(1-\gamma)\ddot{\boldsymbol{p}}^n + \Delta t\, \gamma \ddot{\boldsymbol{p}}^{(n+1)}, \tag{6}$$

where Δt is the time interval between $t = n\Delta t$ and $t = (n+1)\Delta t$, and γ and β are parameters that are related, respectively, to the accuracy and stability of the method. Commonly, γ is set to $1/2$ to maintain second-order accuracy and to eliminate the dissipation error. Then, substitution of Eqs. (5) and (6) into Eq. (1) yields the following linear system of equations:

$$\left[\boldsymbol{M} + \beta\Delta t^2 c^2 \boldsymbol{K} + \frac{c\Delta t}{2}\boldsymbol{C}\right]\ddot{\boldsymbol{p}}^{(n+1)} = \boldsymbol{f}^{(n+1)} - c\boldsymbol{C}\boldsymbol{P} - c^2\boldsymbol{K}\boldsymbol{Q}, \tag{7}$$

where

$$\boldsymbol{f}^{(n+1)} = \rho c^2 \dot{v}_n^{(n+1)} \boldsymbol{W}, \tag{8}$$

$$\boldsymbol{P} = \dot{\boldsymbol{p}}^n + \frac{\Delta t}{2}\ddot{\boldsymbol{p}}^n, \tag{9}$$

$$\boldsymbol{Q} = \boldsymbol{p}^n + \Delta t \dot{\boldsymbol{p}}^n + \left(\frac{1}{2} - \beta\right)\Delta t^2 \ddot{\boldsymbol{p}}^n. \tag{10}$$

By solving Eq. (7) using a direct solver or an iterative solver, $\ddot{\boldsymbol{p}}^{(n+1)}$ is calculable. In this study, as a Krylov subspace iterative method, the conjugate gradient iterative solver with a diagonal scaling preconditioning is applied to solve the equation. Finally, $\boldsymbol{p}^{(n+1)}$ and $\dot{\boldsymbol{p}}^{(n+1)}$ are calculable, respectively, by substituting $\ddot{\boldsymbol{p}}^{(n+1)}$ into Eqs. (5) and (6).

The following implicit Newmark β methods with different parameters β are well known:[15] Constant average acceleration method with $\beta = 1/4$ (CAA), linear acceleration method with $\beta = 1/6$ (LA), and the Fox–Goodwin method with $\beta = 1/12$ (FG). Here, if $\beta \geq 1/4$, then the Newmark method is unconditionally stable. Otherwise the method is conditionally stable and the stability condition, which gives the critical time interval, Δt_{crit}, is given as

$$\Delta t_{\mathrm{crit}} \leq \frac{1}{\omega_{\max}\sqrt{1/4 - \beta}}. \tag{11}$$

Here $\omega_{\max}$ is the maximum natural frequency, which is obtainable by solving generalized eigenvalue problem $(\boldsymbol{k}_e - k^2\boldsymbol{m}_e)\boldsymbol{p}_e = 0$ for all elements.

B. Modified integration rules

To increase the accuracy of four-node quadrilateral FEs for transient acoustic analysis in two dimensions, Yue and Guddati proposed MIR,[12] which is summarized briefly here. Although MIR is proposed for both the implicit Newmark β method and the explicit central difference method, this paper presents specific examination only of the implicit Newmark β method.

In the numerical integration of element stiffness and mass matrices in Eqs. (2) and (3) for four-node quadrilateral isoparametric element, the Gauss quadrature rule with two integration points in each direction is commonly used as

$$\boldsymbol{k}_e \simeq \sum_{i=1}^{4} W_i \boldsymbol{\nabla N}(\alpha_{k,i}, \alpha_{k,i})^T \boldsymbol{\nabla N}(\alpha_{k,i}, \alpha_{k,i}) \det(\mathbf{J}), \tag{12}$$

$$\boldsymbol{m}_e \simeq \sum_{i=1}^{4} W_i \boldsymbol{N}(\alpha_{m,i}, \alpha_{m,i})^T \boldsymbol{N}(\alpha_{m,i}, \alpha_{m,i}) \det(\mathbf{J}), \tag{13}$$

where $\alpha_{k,i}$ and $\alpha_{m,i}$ are coordinates of the ith integration point for $\boldsymbol{k}_e$ and $\boldsymbol{m}_e$, W_i is the weight of ith integration points, $\mathbf{J}$ is the Jacobian matrix. For the conventional Gauss quadrature rule, $\alpha_{k,i} = \alpha_{m,i} = \pm 1/\sqrt{3}$ and $W_i = 1$.

For MIR,[12] integration points are shifted from conventional points to

$$\alpha_{k,i} = \pm\sqrt{\frac{2}{3}}, \quad \alpha_{m,i} = \pm\sqrt{\frac{2}{3} + \left(\frac{1}{3} - 4\beta\right)\frac{c^2\Delta t^2}{h^2}}, \tag{14}$$

where h signifies the size of the square element. With the modification, fourth-order accuracy in dispersion error is achieved as opposed to second-order accuracy in the conventional Gauss rule. However, Eq. (14) is developed for square mesh only. The quantity equivalent to h, and hence the parameter $\alpha_{m,i}$, will depend on the direction of wave propagation for a rectangular or distorted element. Further, as another feature of the MIR, stability conditions of LA and FG are relaxed, although the unconditional stability of CAA is lost.[12]

III. DISPERSION ERROR ANALYSIS

A. Derivation of dispersion relation

Dispersion error analysis in three dimensions is performed to evaluate the dispersion error in time-domain finite-element analysis with eight-node hexahedral linear elements. The analysis follows the same procedure using the following linear multistep form without the source and dissipation terms presented in Ref. 12:

$$(\boldsymbol{M} + \beta\Delta t^2 c^2 \boldsymbol{K})\boldsymbol{p}^{(n+1)} + [-2\boldsymbol{M} + (1-2\beta)\Delta t^2 c^2 \boldsymbol{K}]\boldsymbol{p}^n + (\boldsymbol{M} + \beta\Delta t^2 c^2 \boldsymbol{K})\boldsymbol{p}^{(n-1)} = 0. \tag{15}$$

Equation (15) is based on Ref. 16, which presents a general recurrence relation among $\boldsymbol{p}^{(n+1)}$, $\boldsymbol{p}^{(n)}$, and $\boldsymbol{p}^{(n-1)}$ as

$$\begin{aligned}&(\boldsymbol{M} + \gamma\Delta t c\boldsymbol{C} + \beta\Delta t^2 c^2 \boldsymbol{K})\boldsymbol{p}^{(n+1)} \\ &+ [-2\boldsymbol{M} + (1-2\gamma)\Delta t c\boldsymbol{C} + \left(\frac{1}{2} + \gamma - 2\beta\right)\Delta t^2 c^2 \boldsymbol{K}]\boldsymbol{p}^n \\ &+ [\boldsymbol{M} + (-1+\gamma)\Delta t c\boldsymbol{C} + \left(\frac{1}{2} + \gamma - 2\beta\right)\Delta t^2 c^2 \boldsymbol{K}]\boldsymbol{p}^{(n-1)} \\ &+ \beta\Delta t^2 \boldsymbol{f}^{(n+1)} + \left(\frac{1}{2} + \gamma - 2\beta\right)\Delta t^2 \boldsymbol{f}^n \\ &+ \left(\frac{1}{2} + \gamma - 2\beta\right)\Delta t^2 \boldsymbol{f}^{(n-1)} = 0.\end{aligned} \tag{16}$$

For $\gamma = 1/2$, Eq. (15) is obtainable by neglecting source and dissipation terms from Eq. (16).

In a spherical coordinate system, the solution is a plane wave of the form $\exp[i(kx\sin\theta\cos\phi + ky\sin\theta\sin\phi + kz\cos\theta - \omega t)]$, where i, k, ω, θ, and ϕ, respectively, denote an imaginary unit, wave number, and angular frequency, azimuth, and elevation. Meanwhile, the approximate solution, $\boldsymbol{p}^n_{x,y,z}$ at time $n\Delta t$ and location (x, y, z) is given as

$$\boldsymbol{p}^n_{x,y,z} = \exp[i(k^h x\sin\theta\cos\phi + k^h y\sin\theta\sin\phi + k^h z\cos\theta - \omega^h n\Delta t)], \tag{17}$$

where k^h and ω^h, respectively, denote the approximate wave number and approximate angular frequency. Further, dispersion error, e_{dis}, is defined as

$$e_{\text{dis}} = \frac{|c - c^h|}{c}, \tag{18}$$

where c^h is approximate speed of sound.

To evaluate the dispersion error, a region that consists of eight elements with an eight-node linear element of size $d_x \times d_y \times d_z$ as shown in Fig. 1 is considered. The dispersion error can be evaluated by constructing the FE equation of Eq. (15) at a center node (x, y, z). In Eq. (15) the element mass matrix $\boldsymbol{m}_e$ and stiffness matrix $\boldsymbol{k}_e$, which are calculated using the Gauss quadrature rule in three dimensions with two integration points in each direction are given as

$$\boldsymbol{m}_e = \begin{pmatrix} m_0 & m_x & m_{xy} & m_y & m_z & m_{zx} & m_{xyz} & m_{yz} \\ & m_0 & m_y & m_{xy} & m_{zx} & m_z & m_{yz} & m_{xyz} \\ & & m_0 & m_x & m_{xyz} & m_{yz} & m_z & m_{zx} \\ & & & m_0 & m_{yz} & m_{xyz} & m_{zx} & m_z \\ & & & & m_0 & m_x & m_{xy} & m_y \\ & & & & & m_0 & m_y & m_{xy} \\ & & & & & & m_0 & m_x \\ & \text{sym} & & & & & & m_0 \end{pmatrix}, \tag{19}$$

$$\boldsymbol{k}_e = \begin{pmatrix} k_0 & k_x & k_{xy} & k_y & k_z & k_{zx} & k_{xyz} & k_{yz} \\ & k_0 & k_y & k_{xy} & k_{zx} & k_z & k_{yz} & k_{xyz} \\ & & k_0 & k_x & k_{xyz} & k_{yz} & k_z & k_{zx} \\ & & & k_0 & k_{yz} & k_{xyz} & k_{zx} & k_z \\ & & & & k_0 & k_x & k_{xy} & k_y \\ & & & & & k_0 & k_y & k_{xy} \\ & & & & & & k_0 & k_x \\ & \text{sym} & & & & & & k_0 \end{pmatrix}. \tag{20}$$

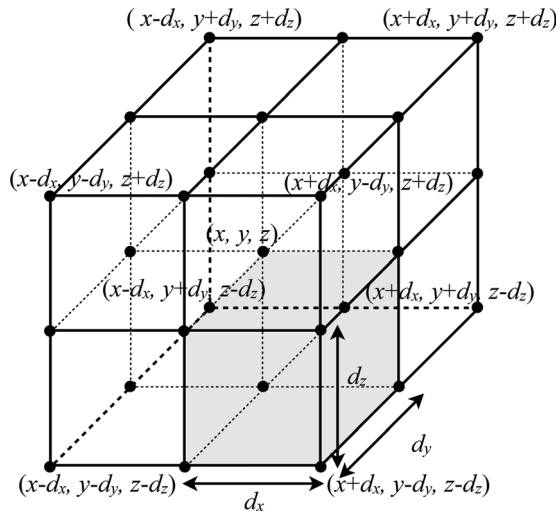

FIG. 1. Twenty-seven-node eight cubic element patch for dispersion error analysis in three dimensions.

Using the $\boldsymbol{m}_e$ and $\boldsymbol{k}_e$, Eq. (15) is calculated for the center node. Then, substituting Eq. (17) into the resulting equation [Eq. (15) for the center node after substituting components of $\boldsymbol{m}_e$ and $\boldsymbol{k}_e$] leads to

$$\begin{aligned}&2(C_t-1)(m_0+m_xC_x+m_yC_y+m_zC_z\\&+m_{xy}C_{xy}+m_{yz}C_{yz}+m_{zx}C_{zx}+m_{xyz}C_{xyz})\\&+c^2\Delta t^2(2\beta C_t+1-2\beta)(k_0+k_xC_x+k_yC_y+k_zC_z\\&+k_{xy}C_{xy}+k_{yz}C_{yz}+k_{zx}C_{zx}+k_{xyz}C_{xyz})=0,\end{aligned}\tag{21}$$

where

$$\begin{aligned}&C_x=\cos(k^hd_x\sin\theta\cos\phi),\ C_y=\cos(k^hd_y\sin\theta\sin\phi)\\&C_z=\cos(k^hd_z\cos\theta),\ C_t=\cos(c^hk^h\Delta t),\ C_{xy}=C_xC_y\\&C_{yz}=C_yC_z,\ C_{zx}=C_zC_x,\ C_{xyz}=C_xC_yC_z.\end{aligned}\tag{22}$$

From Eq. (21), the relation between the exact speed of sound c and the approximate speed of sound c^h becomes

$$c=\frac{1}{\Delta t}\left[\frac{2(1-C_t)(m_0+m_xC_x+m_yC_y+m_zC_z+m_{xy}C_{xy}+m_{yz}C_{yz}+m_{zx}C_{zx}+m_{xyz}C_{xyz})}{(2\beta C_t+1-2\beta)(k_0+k_xC_x+k_yC_y+k_zC_z+k_{xy}C_{xy}+k_{yz}C_{yz}+k_{zx}C_{zx}+k_{xyz}C_{xyz})}\right]^{1/2}.\tag{23}$$

Using Taylor expansion with respect to k^h, the dispersion error e_{dis} can be evaluated as

$$\begin{aligned}e_{\text{dis}}\simeq&\frac{k^2}{24}[\chi_xd_x^2+\chi_yd_y^2+\chi_zd_z^2-(1-12\beta)c^2\Delta t^2]\\&+O[k^4(d_x^4+d_y^4+d_z^4)+(c\Delta t)^4],\end{aligned}\tag{24}$$

where

$$\begin{aligned}\chi_x=&(3\alpha_m^2-2)\cos^4\phi\sin^4\theta-3(\alpha_k^2-\alpha_m^2)\\&\times(\cos^2\theta\sin^2\theta\cos^2\phi+\cos^2\phi\sin^2\phi\sin^4\theta),\\\chi_y=&(3\alpha_m^2-2)\sin^4\phi\sin^4\theta-3(\alpha_k^2-\alpha_m^2)\\&\times(\cos^2\theta\sin^2\theta\sin^2\phi+\cos^2\phi\sin^2\phi\sin^4\theta),\\\chi_z=&(3\alpha_m^2-2)\cos^4\theta-3(\alpha_k^2-\alpha_m^2)\cos^2\theta\sin^2\theta.\end{aligned}\tag{25}$$

Equation (24) in three dimensions is similar to Eq. (13) of Ref. 12 in two dimensions. The three-dimensional equation can be reduced to the two-dimensional one by transforming a spherical coordinate system into a two-dimensional polar coordinate system.

For the conventional Gauss rule, the dispersion error of Eq. (24) becomes

$$\begin{aligned}e_{\text{dis}}\simeq&\frac{k^2}{24}[d_x^2\cos^4\phi\sin^4\theta+d_y^2\sin^4\phi\sin^4\theta+d_z^2\cos^4\theta\\&+(1-12\beta)c^2\Delta t^2]+O[k^4(d_x^4+d_y^4+d_z^4)+(c\Delta t)^4].\end{aligned}\tag{26}$$

The order of error is of second order. Meanwhile, the second-order error term in Eq. (26) can be eliminated using MIR, which is defined as

$$\alpha_{k,i}=\pm\sqrt{\frac{2}{3}},\quad \alpha_{m,i}=\pm\sqrt{\frac{2}{3}+\left(\frac{1}{3}-4\beta\right)\frac{c^2\Delta t^2}{\tau}},\tag{27}$$

where

$$\tau=d_x^2\cos^2\phi\sin^2\theta+d_y^2\sin^2\phi\sin^2\theta+d_z^2\cos^2\theta.\tag{28}$$

In the above-presented equation, $\alpha_{m,i}$ depends on the direction of wave propagation, i.e., ϕ and θ in τ. For CAA and LA, the values of τ cannot be determined uniquely for a rectangular element unless the values of ϕ and θ are determined at one direction. Consequently, the second-order error term cannot be eliminated for a rectangular element. For a cubic element (i.e., $d_x=d_y=d_z=h$), the value of τ is determined uniquely as $\tau=h^2$. The second-order error term can be eliminated, as shown in Ref. 12. However, using FG, $\alpha_{m,i}$ is determined uniquely as $\pm\sqrt{2/3}$, without depending on the direction of wave propagation even for a rectangular element because the last term in the square root in Eq. (27) becomes zero if β is exactly 1/12, as in FG. In this case, MIR can markedly reduce the dispersion error even for a non-cubic (rectangular) element. Although the integration points for FG are already pointed out in Sec. III C. of Ref. 12, this special case is not described explicitly. Consequently, the dispersion error for FG with MIR is

$$\begin{aligned}e_{\text{dis.}}\simeq&\frac{k^4}{480}[d_x^4\cos^6\phi\sin^6\theta+d_y^4\sin^6\phi\sin^6\theta+d_z^4\cos^6\theta-c^4\Delta t^4]\\&+O[k^6(d_x^6+d_y^6+d_z^6)+(c\Delta t)^6].\end{aligned}\tag{29}$$

The order of error becomes fourth-order, which is two orders of magnitude smaller than the conventional rule in Eq. (26). Using Eqs. (26) and (29), the dispersion error in FE analysis using an eight-node hexahedral linear element can be estimated with various element sizes and time intervals.

B. Stability condition

The stability condition of Eq. (11) for TD-FEM with MIR using rectangular eight-node hexahedral elements and the difference of the conditions between two- and three-dimensional analyses are shown here. By solving the generalized eigenvalue problem $(\boldsymbol{k}_e-k^2\boldsymbol{m}_e)\boldsymbol{p}_e=0$ with $\alpha_k=\sqrt{2/3}$, $\omega_{\max}$ of Eq. (11) for three-dimensional analysis using rectangular elements is given as

$$\omega_{\max} = \max\left[\frac{2c}{d_x\alpha_m}, \frac{2c}{d_y\alpha_m}, \frac{2c}{d_z\alpha_m}, \frac{c}{\alpha_m^2}\sqrt{\frac{8}{3}\left(\frac{1}{d_x^2}+\frac{1}{d_y^2}\right)}, \frac{c}{\alpha_m^2}\sqrt{\frac{8}{3}\left(\frac{1}{d_y^2}+\frac{1}{d_z^2}\right)}, \frac{c}{\alpha_m^2}\sqrt{\frac{8}{3}\left(\frac{1}{d_z^2}+\frac{1}{d_x^2}\right)}, \frac{4c}{3\alpha_m^3}\sqrt{\left(\frac{1}{d_x^2}+\frac{1}{d_y^2}+\frac{1}{d_z^2}\right)}\right]. \quad (30)$$

Consequently, for FG with MIR, the stability condition is

$$\Delta t \le \min\left[\frac{d_x}{c}, \frac{d_y}{c}, \frac{d_z}{c}, \frac{1}{c\sqrt{\frac{1}{d_x^2}+\frac{1}{d_y^2}}}, \frac{1}{c\sqrt{\frac{1}{d_y^2}+\frac{1}{d_z^2}}}, \frac{1}{c\sqrt{\frac{1}{d_z^2}+\frac{1}{d_x^2}}}, \frac{1}{c\sqrt{\frac{1}{d_x^2}+\frac{1}{d_y^2}+\frac{1}{d_z^2}}}\right]. \quad (31)$$

Meanwhile, the $\omega_{\max}$ for rectangular elements with conventional Gauss rule is given as

$$\omega_{\max} = \max\left[\frac{2\sqrt{3}c}{d_x}, \frac{2\sqrt{3}c}{d_y}, \frac{2\sqrt{3}c}{d_z}, 2\sqrt{3}c\sqrt{\left(\frac{1}{d_x^2}+\frac{1}{d_y^2}\right)}, 2\sqrt{3}c\sqrt{\left(\frac{1}{d_y^2}+\frac{1}{d_z^2}\right)}, 2\sqrt{3}c\sqrt{\left(\frac{1}{d_z^2}+\frac{1}{d_x^2}\right)}, 2\sqrt{3}c\sqrt{\left(\frac{1}{d_x^2}+\frac{1}{d_y^2}+\frac{1}{d_z^2}\right)}\right]. \quad (32)$$

Consequently, stability condition for FG with conventional Gauss rule is

$$\Delta t \le \min\left[\frac{d_x}{\sqrt{2}c}, \frac{d_y}{\sqrt{2}c}, \frac{d_z}{\sqrt{2}c}, \frac{1}{\sqrt{2}c\sqrt{\frac{1}{d_x^2}+\frac{1}{d_y^2}}}, \frac{1}{\sqrt{2}c\sqrt{\frac{1}{d_y^2}+\frac{1}{d_z^2}}}, \frac{1}{\sqrt{2}c\sqrt{\frac{1}{d_z^2}+\frac{1}{d_x^2}}}, \frac{1}{\sqrt{2}c\sqrt{\frac{1}{d_x^2}+\frac{1}{d_y^2}+\frac{1}{d_z^2}}}\right]. \quad (33)$$

From Eqs. (31) and (33), it is confirmed that the stability condition of FG with MIR in three dimensions is also relaxed using MIR, as shown in Ref. 12. Further, the $\omega_{\max}$ for cubic elements with MIR becomes

$$\omega_{\max} = \max\left(\frac{2c}{h\alpha_m}, \frac{4c}{\sqrt{3}h\alpha_m^2}, \frac{4c}{\sqrt{3}h\alpha_m^3}\right). \quad (34)$$

Compared to $\omega_{\max}$ for two-dimensional analysis using square elements[12] (i.e., $\omega_{\max} = \max[2c/(h\alpha_m), 4c/(\sqrt{3}h\alpha_m^2)]$), a new eigenvalue $4c/(\sqrt{3}h\alpha_m^3)$ appears in three-dimensional analysis using cubic elements. From the result, the value of Δt to satisfy the stability condition in three-dimensional analysis differs from that of two-dimensional analysis.

C. Comparison of dispersion error

To confirm the difference of accuracy between the conventional rule and MIR, the dispersion errors at all directions of wave propagation calculated using Eqs. (26) and (29) are compared. In those calculations, $k = 9\pi/2$, $c = 343.7$ m/s, and $\Delta t = 1/16\,384$ s are considered. The element size is $d_x = 0.1$ m, $d_y = 0.09$ m, and $d_z = 0.06$ m. Newmark methods of three types (CAA, LA, and FG) are used in the calculation of Eq. (26).

Figures 2(a)–2(d) present a comparison of dispersion errors at all directions of wave propagation in CAA, LA, and FG with the conventional Gauss rule and FG with MIR. Results show that FG with MIR performs much better than other conventional methods with smaller dispersion error at all propagation directions. The maximum error of FG with MIR is 0.83% at $(\theta, \phi) = (90°, 0°)$ and the errors of other conventional methods are, respectively, 7.60% (CAA), 7.96% (LA), and 8.33% (FG) at $(\theta, \phi) = (90°, 0°)$. The reason underlying the maximum error at $(\theta, \phi) = (90°, 0°)$ is that the element size of x-direction (i.e., d_x) is the longest.

To show other aspects of dispersion error for FG with MIR, the relation between dispersion error and λ/d_x at $(\theta, \phi) = (90°, 0°)$, where λ is wavelength, is shown in

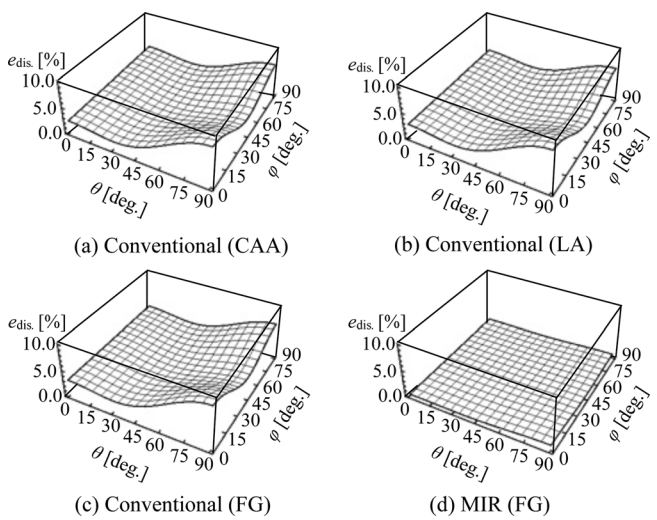

(a) Conventional (CAA) (b) Conventional (LA)

(c) Conventional (FG) (d) MIR (FG)

FIG. 2. Comparison of dispersion errors at all directions of wave propagation among various Newmark β methods with conventional Gauss rule and with MIR: (a) CAA with conventional rule, (b) LA with conventional rule, (c) FG with conventional rule, and (d) FG with MIR.

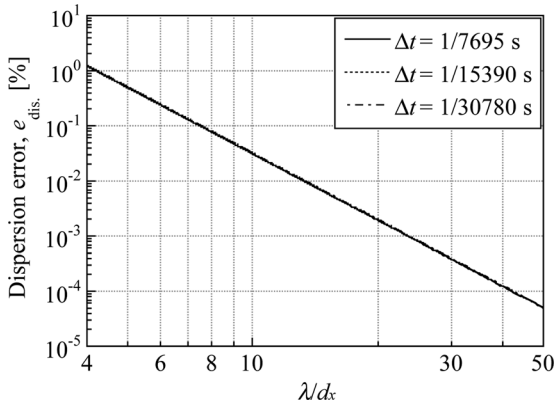

FIG. 3. Relations between dispersion errors and nodal distance per wavelength, λ/d_x, at $(\theta, \phi) = (90°, 0°)$ of FG with MIR at different time intervals.

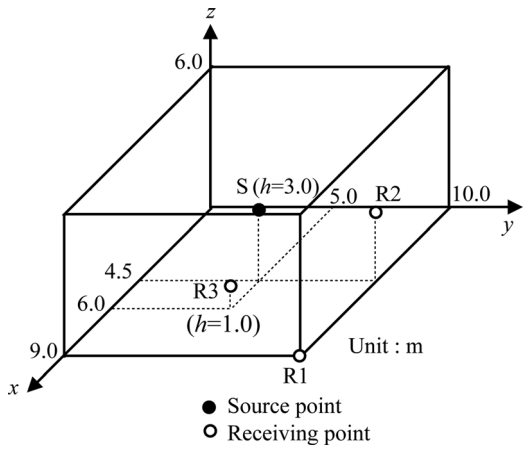

FIG. 4. Rectangular room to be analyzed.

Fig. 3. Here, the angle occurring with maximum error is selected to estimate the error on the safe side. Then we consider Δt_{crit} of three kinds, which are 1/7695, 1/15 390, and 1/30 780 s. The largest Δt is slightly lower than Δt_{crit}, which is 1/7694.8 s for a given element. The others are, respectively, one-half and one-quarter of Δt_{crit}. Results show that the errors become almost equal even if a smaller time interval is used. Therefore, the use of a slightly lower time interval than Δt_{crit} is beneficial for efficient computation.

IV. NUMERICAL EXPERIMENTS

In the dispersion analysis described in Sec. III, we assumed that the use of rectangular elements in free space, and MIR are therefore not strictly applicable to analyses with distorted elements and with impedance boundary conditions. In addition, the source term is not considered. Therefore, the accuracy and efficiency of FG with MIR for these conditions are examined using three numerical experiments. First, we consider a problem with a source term to confirm the finding of the previous section numerically. Then problems with distorted elements and finite impedance boundary conditions are regarded as more general problems. For all numerical experiments, we assume that $c = 343.7$ m/s and $\rho = 1.205$ kg/m^3.

A. Source term

The sound field in a rectangular room with acoustically hard surfaces is analyzed using FG with MIR and with a conventional Gauss rule, the results are compared with the analytical solution (method of variable separation)[17] with a Gaussian pulse. Figure 4 portrays the analyzed room with volume of 540 m^3. We calculate the sound pressures at three receiving points radiated from a sound source as shown in Fig. 4. The sound source used here is a modulated Gaussian pulse, which is also used for subsequent numerical experiments. Its waveform and frequency characteristics are depicted in Fig. 5. The upper limit frequency is assumed as 682 Hz that has −3 dB gain. In Ref. 17, this sound source is presented as a sound source of spatial distribution type. The analytical solution used here is derived using the Gaussian pulse as an initial condition. Meanwhile, the temporal source function is generally used for TD-FEM, which is given as a volume acceleration waveform. Consequently, the transformation process from spatial distribution to a temporal distribution is necessary and the transformation is conducted as follows. The Gaussian pulse[17] is defined as $p(r) = \exp(-r^2/d^2)$, where r is the distance from the source and d is a constant. Considering propagation of a spherical wave in a free field, the analytical solution for sound pressure, $p(r,t)$, is given as[17]

$$p(r,t) = \frac{1}{2r}(r - ct)e^{-(r-ct)^2/d^2}, \tag{35}$$

where only the outgoing wave is shown. The relation between $p(r,t)$ and the volume velocity of sound source Q is given as[18]

$$p(r,t) = \frac{\rho}{4\pi r}\dot{Q}\left(t - \frac{r}{c}\right). \tag{36}$$

Using this relation, the volume acceleration waveform is calculated. Here, $d = 0.218$ is used. However, using this relation, the time lag of r/c s occurs between the FE solution and an analytical solution. Therefore, we shifted the origin of the temporal axis of the FE solution from $t = 0$ s to $t = r/c$ s for comparison.

For spatial discretization, three meshes with different spatial resolutions are created and the respective spatial resolutions $\lambda/d_{\max}$ are 6.1, 12.1, and 18.1, where λ and $d_{\max}$,

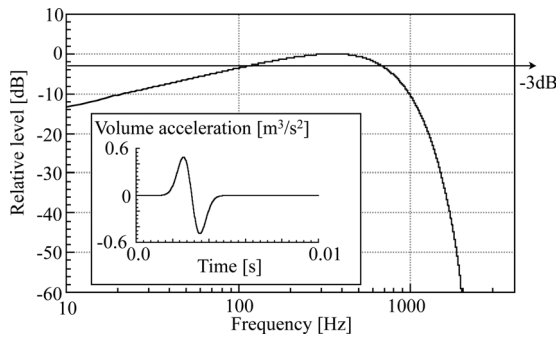

FIG. 5. Volume acceleration waveform and its frequency characteristics of Gaussian pulse as a sound source for time-domain finite-element analysis.

respectively, denote the wavelength of the upper limit frequency and maximum nodal distance. The DOFs of these meshes are, respectively, 1 771 561, 13 997 521, and 47 045 881. The critical time intervals of FG with MIR for each mesh are, respectively, 1/9234, 1/18 468, and 1/27 701 s. For the conventional Gauss rule, the values are, respectively, 1/13 059, 1/26 117, and 1/39 176 s. The sound pressure is calculated up to 200 ms with $\Delta t = 1/28\,000$ s for MIR and 1/40 000 s for a conventional rule. They are determined to satisfy the stability conditions for the finest mesh. The stopping criterion of the conjugate gradient method is used as

$$\frac{\|\boldsymbol{A}\ddot{\boldsymbol{p}}_j^{(n+1)} - \boldsymbol{b}^{(n+1)}\|_2}{\|\boldsymbol{b}^{(n+1)}\|_2} \leq 10^{-6}, \tag{37}$$

where $\boldsymbol{A}$, $\ddot{\boldsymbol{p}}_j^{(n+1)}$, and $\boldsymbol{b}$, respectively denote the coefficient matrix, solution vector on jth iteration, and right-hand side vector in Eq. (7). This criterion is also used for subsequent experiments.

Figure 6 presents comparisons of waveforms at a receiving point R3 obtained by FG with both integration rules for mesh with $\lambda/d_{\max} > 6.1$ and using analytical method. The fine structure of the waveform by FG with MIR agrees well with an analytical solution, and the agreement is much better than that between the solution by FG with the conventional rule and the analytical solution. Further, the error in sound pressure of entire time range analyzed is measured as the relative error defined by

$$e_p = \frac{1}{N_{\text{step}}} \sum_{j=1}^{N_{\text{step}}} e(t_j), \tag{38}$$

with

$$e(t) = \sqrt{\frac{\sum_{i=1}^{N} [p_{\text{ana}}(\boldsymbol{x}_i, t) - p_{\text{FEM}}(\boldsymbol{x}_i, t)]^2}{\sum_{i=1}^{N} p_{\text{ana}}(\boldsymbol{x}_i, t)^2}}, \tag{39}$$

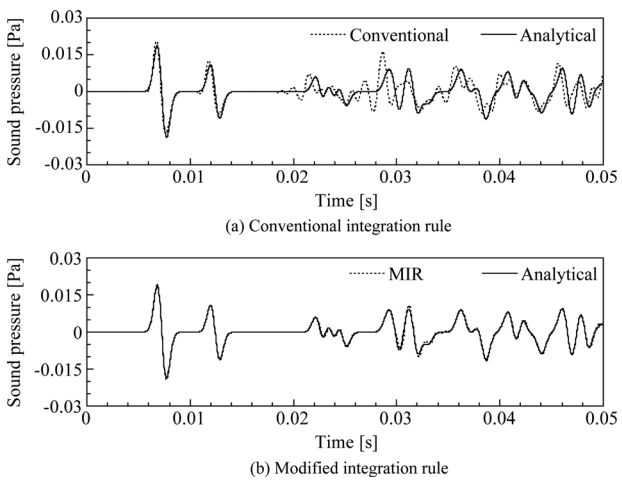

FIG. 6. Comparisons of sound pressure waveforms at a receiving point R3 obtained using (a) FG with a conventional Gauss rule and obtained using an analytical method and (b) FG with MIR and obtained using an analytical method.

where $p_{\text{ana}}(\boldsymbol{x}_i, t)$ and $p_{\text{FEM}}(\boldsymbol{x}_i, t)$, respectively, denote sound pressures at receiving point $\boldsymbol{x}_i$ at time t obtained using the analytical method and FG with both integration rules. N and N_{step}, respectively, denote the number of receiving points and the total number of time step.

Figure 7 presents relations between the relative error in sound pressure e_p and nodal distance per wavelength for FG with MIR and conventional rules. Results show that the errors of FG with MIR are much lower than those of FG with conventional rules. Moreover, the reduction rate of errors of the FG with MIR follows a theoretical slope.

Further, to present other advantages of the use of MIR, the convergence properties of an iterative solver using both integration rules for each mesh are presented in Fig. 8, which shows the mean quantity of iterations of diagonal scaled conjugate gradient method required for convergence at each time step. Clearly, the numbers of iterations of MIR are less than those of the conventional Gauss rule for all meshes. Although direct comparison of computational cost is difficult because the accuracy of waveforms obtained by both integration rules differs, the reduction rate of the number of iterations, R_N, using MIR for each mesh are 34.1% ($\lambda/d_{\max} > 6.1$), 46.6% ($\lambda/d_{\max} > 12.1$), and 56.8% ($\lambda/d_{\max} > 18.1$), which means that the computational time of MIR is at least 34.1% shorter than that of the conventional Gauss rule for problems with same degrees of freedom. Here, R_{N} defined as $R_{\text{N}} = (N_{\text{Conv}} - N_{\text{MIR}})/N_{\text{Conv}} \times 100(\%)$, where N_{Conv} and N_{MIR}, respectively, denote the mean numbers of iterations per time step for the conventional Gauss rule and MIR.

B. Distorted element

As described previously, the presented dispersion analysis is based on the use of rectangular elements. However, FG with MIR might be applicable to analysis using distorted elements because $\alpha_{m,i}$ of FG with MIR has no parameter in terms of element size, which is confirmed here. The sound field in a rectangular room of 120 m^3 with acoustically hard surfaces as shown in Fig. 9 is analyzed using FG with both integration rules. The results are compared with the analytical solution. Here, the room is discretized using distorted elements. The sound pressures at five receiving points are

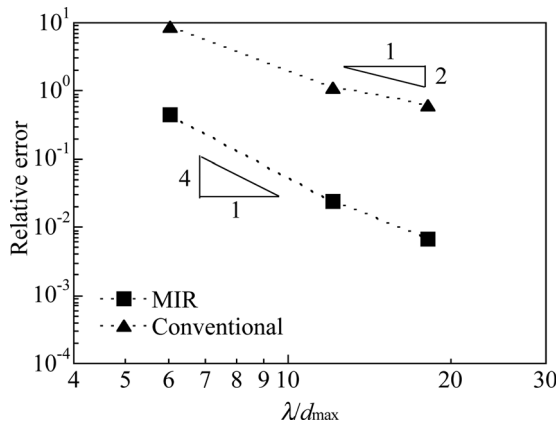

FIG. 7. Relation between relative error in sound pressure and nodal distance per wavelength, $\lambda/d_{\max}$, for FG with MIR and conventional rule.

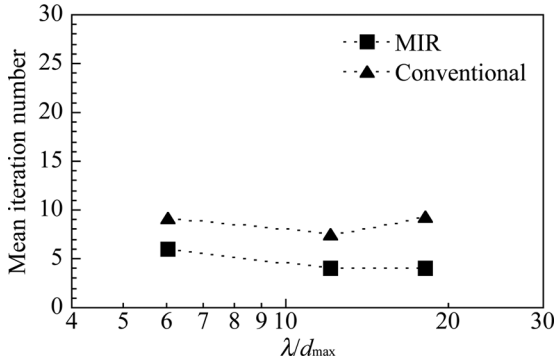

FIG. 8. Comparisons of mean iteration numbers per time step of diagonal scaled conjugate gradient method for both integration rules.

calculated using FG with both integration rules for three meshes with $\lambda/d_{\max} > 6.0$, 12.1, and 24.2 that consist of distorted elements. These meshes including distorted elements are created by discretizing side AI, IB, DJ, JC, EK, KF, HL, and LG with n_y elements in the y direction. We used $n_y = 42$, 84, and 168 elements, respectively, for meshes with $\lambda/d_{\max} > 6.0$, 12.1, and 24.2. For x and z directions, we used 72, 144, and 288 elements, respectively. The DOFs of these meshes are, respectively, 452 965, 3 553 225, and 28 146 577.

The sound pressure is calculated up to 200 ms with $\Delta t = 1/40\,000$ s for FG with MIR and with $\Delta t = 1/57\,000$ s for FG with conventional rule. Here, these Δt's are determined to satisfy the stability condition for the finest mesh. The Δt_{crit}'s for both integration rules are, respectively, 1/39 636.8 s (MIR) and 1/56 054.9 s (conventional).

Figure 10 presents relations between the relative error in sound pressure e_p and nodal distance per wavelength for FG with MIR and conventional rules. It is observed that FG with MIR has second-order accuracy for distorted elements, but the errors of FG with MIR are much lower than those of FG with conventional rules. For meshes with $\lambda/d_{\max} > 12.1$ and 24.2, the errors of FG with MIR are 1 order of magnitude

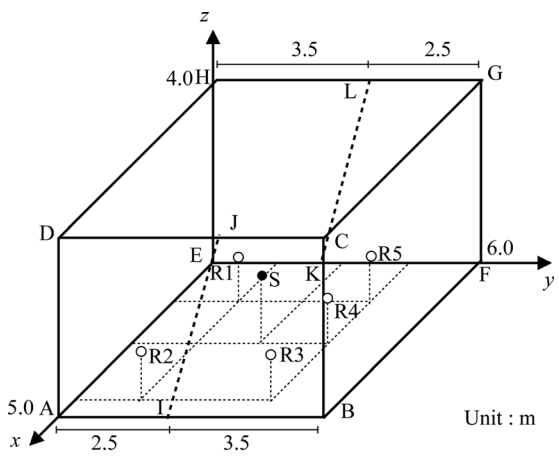

Coordinates of source point, S and receiving points, R1~R5.

S : (2.5, 2.875, 1.5)	R3 : (4.375, 4.375, 1.0)
R1 : (1.25, 1.375, 1.0)	R4 : (2.5, 4.375, 1.0)
R2 : (4.375, 1.375, 1.0)	R5 : (1.25, 4.375, 1.0)

FIG. 9. Rectangular room to be analyzed for the distorted elements case.

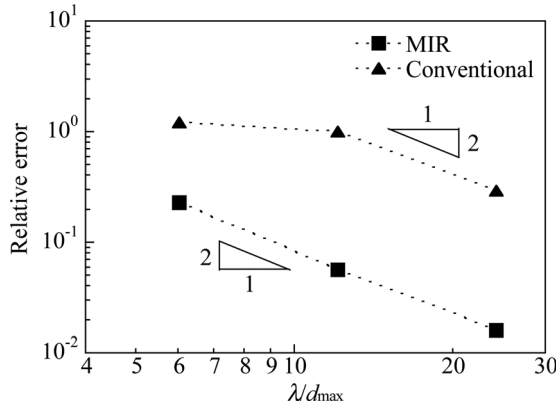

FIG. 10. Relation between relative error in sound pressure and nodal distance per wavelength, $\lambda/d_{\max}$, for FG with MIR and conventional rule (distorted elements case).

smaller than those of FG with conventional rules. As the results show, it can be inferred that element shape does not hugely affect the applicability of FG with MIR by eliminating the term of element sizes, i.e., d_x, d_y, and d_z in $\alpha_{m,i}$.

Further, the mean iteration numbers of the diagonal scaled conjugate gradient method for both integration rules are presented in Fig. 11. For the use of distorted elements, the number of iterations of MIR is also less than those of the conventional Gauss rule for a problem with equal DOF. The reduction rate of the number of iterations, R_N, using MIR for each mesh are 40.6% ($\lambda/d_{\max} > 6.1$), 42.3% ($\lambda/d_{\max} > 12.1$), and 61.7% ($\lambda/d_{\max} > 24.2$). Although more systematic investigation is necessary to reveal the actual accuracy of FG with MIR for distorted elements, it is confirmed that FG with MIR fundamentally performs better than the conventional one, even for the distorted elements.

C. Finite impedance boundary condition

The sound field in an irregularly shaped room of 170.1 m^3 with finite impedance boundary conditions as shown in Fig. 12 is calculated using FG with MIR and with a conventional Gauss rule for three meshes with different spatial resolutions. The results are compared with reference solution. Here, the solution calculated using FG with MIR for mesh with high spatial resolution $\lambda/d_{\max} > 21.0$ is assumed as a reference solution because MIR basically performs better

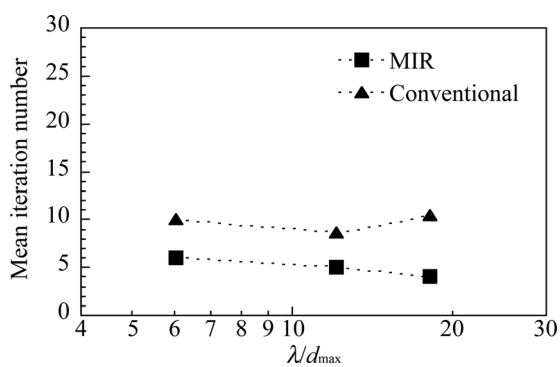

FIG. 11. Comparisons of mean iteration numbers per time step of diagonal scaled conjugate gradient method for both integration rules (distorted elements case).

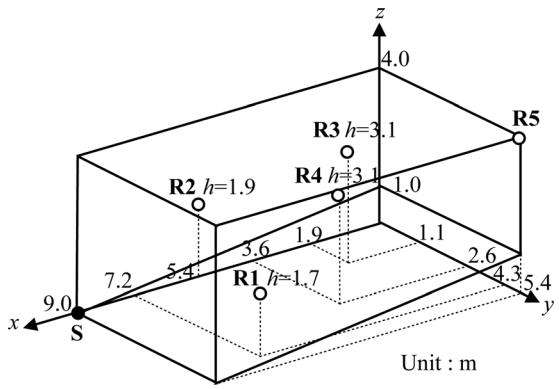

FIG. 12. Irregularly shaped room to be analyzed with a sound source point, S and five receiving points, R1–R5.

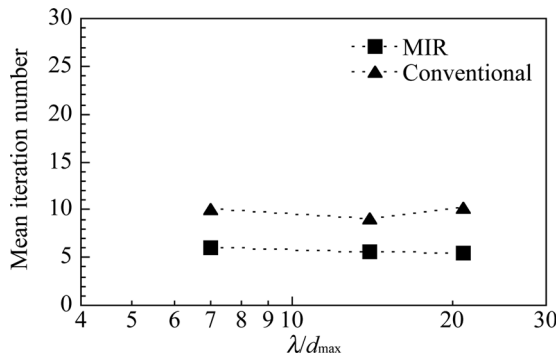

FIG. 14. Comparisons of mean iteration numbers per time step of diagonal scaled conjugate gradient method for both integration rules (finite impedance boundary condition case).

than a conventional Gauss rule, even for distorted elements, as described in a previous section. Including the high-resolution mesh with $\lambda/d_{\max} > 21.0$, we created three meshes, and the remaining two meshes have spatial resolutions of $\lambda/d_{\max} > 7.0$ and 14.0, respectively. The DOFs of these meshes are, respectively, 557 403, 4 374 117, and 14 667 679.

Regarding the boundary condition, the normalized acoustic impedance ratios z_n's corresponding to statistical absorption coefficients α_s's of 0.3 (ceiling), 0.15 (floor), and 0.08 (wall) are given for each boundary. The z_n's are derived from the Paris formula with an assumption that z_n is a real number, which is defined as[19]

$$\alpha_s = \frac{8}{z_n^2}\left[1 + z_n - \frac{1}{1+z_n} - 2\ln(1+z_n)\right]. \tag{40}$$

Further, we assumed that z_n is a frequency independent value in the entire frequency range. With the assumptions, the effect of phase changes and frequency dependence of impedance boundary conditions are not tested here. The reverberation time calculated using Sabine's equation is 0.91 s. Therefore, the sound pressure is calculated up to 1000 ms with $\Delta t = 1/44\,100$ s.

Figure 13 presents the relation between the relative error in sound pressure e_p and nodal distance per wavelength for

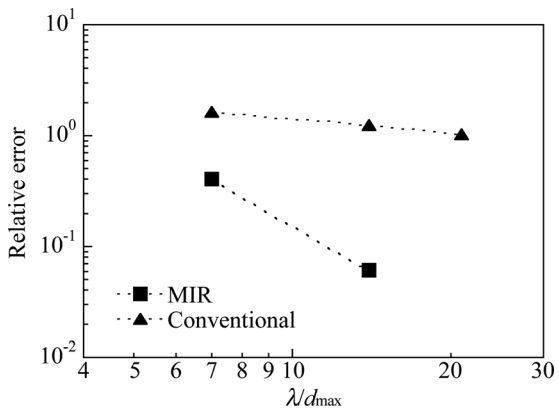

FIG. 13. Relation between the relative error from the reference solution and the nodal distance per wavelength, $\lambda/d_{\max}$, for FG with MIR and the conventional rule (finite impedance boundary case).

FG with MIR and conventional rules. The e_p is calculated using reference solution instead of analytical solution. Therefore, we assume here that results of FG with MIR for mesh with $\lambda/d_{\max} > 21.0$ give the lowest error. Results show that FG with MIR gives lower error than FG with conventional rules for mesh with same DOF. Based on numerical results, the basic effectiveness of MIR for problem with real and frequency-independent finite impedance boundary conditions is confirmed. Finally, mean iteration numbers of diagonal scaled conjugate gradient method for both integration rules are presented in Fig. 14. The mean iteration numbers of diagonal scaled conjugate gradient method with MIR are also less than those with conventional rules, and the R_N for each mesh are 40.4% ($\lambda/d_{\max} > 7.0$), 38.3% ($\lambda/d_{\max} > 14.0$), and 46.5% ($\lambda/d_{\max} > 21.0$), respectively.

V. CONCLUSIONS

To conclude, the applicability of the modified integration rule is tested for sound field analysis of an architectural space using TD-FEM through dispersion error analysis and numerical experiments. First, the dispersion error in finite-element analysis with eight-node hexahedral elements is evaluated through dispersion error analysis in three dimensions, which provides the basis of estimating spatial resolution of a FE mesh and time resolution. Here, the dispersion error analysis in three dimensions is an extension of that in two dimensions described in Ref. 12. The analyses confirmed that using Fox–Goodwin method with the modified integration rule of $\alpha_{k,i} = \alpha_{m,i} = \pm\sqrt{2/3}$, fourth-order accuracy with respect to dispersion error is obtainable even in the use of rectangular elements. The stability condition for three-dimensional analysis using rectangular elements is also shown, and the condition of three-dimensional analysis differs from that of two-dimensional analysis. Then, the accuracy and efficiency of FG with MIR are tested using three numerical examples. From the problem with a source term, we confirmed that FG with MIR has fourth-order accuracy. Numerical evidence also shows that MIR fundamentally performs much better than the conventional Gauss rule, even for a problem with distorted elements, as well as finite impedance boundary conditions (normal acoustic impedance ratio of real and frequency independent values is assumed here).

Further, as another advantage of MIR in computational efficiency, a Krylov subspace iterative method converges more rapidly than a conventional Gauss rule for a problem with the same DOF. The use of FG with MIR engenders efficient computation with fewer DOF than the use of a conventional Gauss rule to obtain results of the same level of accuracy, and enables us to compute problems with larger room volume and/or higher frequencies more efficiently.

ACKNOWLEDGMENT

This research was conducted as one Research Project (A) of the Venture Business Laboratory at Oita University.

[1]D. Botteldooren, "Finite-difference time-domain simulation of low-frequency room acoustic problems," J. Acoust. Soc. Am. **98**(6), 3302–3308 (1995).
[2]J. LoVetri, D. Mardare, and G. Soulodre, "Modeling of the seat dip effect using the finite-difference time-domain method," J. Acoust. Soc. Am. **100**(4), 2204–2212 (1996).
[3]S. Sakamoto, H. Nagatomo, A. Ushiyama, and H. Tachibana, "Calculation of impulse responses and acoustic parameters in a hall by the finite-difference time-domain method," Acoust. Sci. Tech. **29**(4), 256–265 (2008).
[4]A. Craggs, "A finite element method for the free vibration of air in ducts and rooms with absorbing walls," J. Sound Vib. **173**(4), 568–576 (1994).
[5]V. Easwaran and A. Craggs, "Transient response of lightly damped rooms: A finite element approach," J. Acoust. Soc. Am. **99**(1), 108–113 (1996).
[6]N. Okamoto, R. Tomiku, T. Otsuru, and Y. Yasuda, "Numerical analysis of large-scale sound fields using iterative methods part II: Application of Krylov subspace methods to finite element analysis," J. Comput. Acoust. **15**(4), 473–493 (2007).
[7]Y. Yasuda, S. Sakamoto, Y. Kosaka, T. Sakuma, N. Okamoto, and T. Oshima, "Numerical analysis of large-scale sound fields using iterative methods part I: Application of Krylov subspace methods to boundary element analysis," J. Comput. Acoust. **15**(4), 449–471 (2007).
[8]N. M. Newmark, "A method of computation for structural dynamics," J. Eng. Mech. Div. **85**, 67–94 (1959).
[9]T. Otsuru, T. Okuzono, N. Okamoto, K. Isobe, and H. Furuya, "Time domain large-scale finite element sound field analysis of a multi-purpose hall," *Proceedings of the 14th International Congress on Sound and Vibration*, Cairns, Australia, 2007, P440 on CD-ROM.
[10]T. Okuzono, T. Otsuru, R. Tomiku, and N. Okamoto, "Fundamental accuracy of time domain finite element method for sound-field analysis of rooms," Appl. Acoust. **71**(10), 940–946 (2010).
[11]S. Krenk, "Dispersion-corrected explicit integration of the wave equation," Comput. Methods Appl. Mech. Eng. **191**, 975–987 (2001).
[12]B. Yue and M. N. Guddati, "Dispersion-reducing finite elements for transient acoustics," J. Acoust. Soc. Am. **118**(4), 2132–2141 (2005).
[13]T. Otsuru and R. Tomiku, "Basic characteristics and accuracy of acoustic element using spline function in finite element sound field analysis," Acoust. Sci. Tech. **21**(2), 87–95 (2000).
[14]G. Cohen, A. Hauck, M. Kaltenbacher, and T. Otsuru, "Different types of finite elements: Mixed spectral finite elements," in *Computational Acoustics of Noise Propagation in Fluids* edited by S. Marburg and B. Nolte (Springer, Berlin, 2008), Chap. 2.4, pp. 73–84.
[15]T. J. R. Hughes, *The Finite Element Method: Linear Static and Dynamic Finite Element Analysis* (Dover, Mineola, NY, 2000), p. 493.
[16]O. C. Zienkiewicz, "A new look at the Newmark, Houbolt and other time stepping formula. A weighted residual approach," Earthquake Eng. Struct. Dyn. **5**, 413–418 (1977).
[17]S. Sakamoto, "Phase-error analysis of high-order finite difference time domain scheme and its influence on calculation results of impulse response in closed sound field," Acoust. Sci. Tech. **28**(5), 295–309 (2007).
[18]M. Vorländer, *Auralization* (Springer, Berlin, 2008), pp. 23 and 24.
[19]A. London, "The determination of reverberant sound absorption coefficients from acoustic impedance measurements," J. Acoust. Soc. Am. **22**(2), 263–269 (1950).